J. Fluid Mech. (1973), *vol.* 59, *part* 4, *pp.* 693–705
Printed in Great Britain

Pulsating flow in a curved tube

By R. G. ZALOSH
Mt Auburn Research Associates, Inc., Newton Upper Falls, Massachusetts
AND W. G. NELSON
Mechanical Engineering Department, Northeastern University,
Boston, Massachusetts

(Received 12 June 1972 and in revised form 5 March 1973)

An analysis is presented of laminar fully developed flow in a curved tube of circular cross-section under the influence of a pressure gradient oscillating sinusoidally in time. The governing equations are linearized by an expansion valid for small values of the parameter $(a/R)\,[Ka/\omega\nu]^2$, where a is the radius of the tube cross-section, R is the radius of curvature, ν is the kinematic viscosity of the fluid and K and ω are the amplitude and frequency, respectively, of the pressure gradient. A solution involving numerical evaluation of finite Hankel transforms is obtained for arbitrary values of the parameter $\alpha = a(\omega/\nu)^{\frac{1}{2}}$. In addition, closed-form analytic solutions are derived for both small and large values of α. The secondary flow is found to consist of a steady component and a component oscillatory at a frequency 2ω, while the axial velocity perturbation oscillates at ω and 3ω. The small-α flow field is similar to the low Dean number steady flow configuration, whereas the large-α flow field is altered and includes secondary flow directed towards the centre of curvature.

1. Introduction

The steady fully developed flow of a viscous fluid in a curved tube is well understood. The nature of the flow field is characterized by the value of the Dean number $D = (a/R)^{\frac{1}{2}}Re$, where a is the radius of the tube cross-section, R is the radius of curvature of the tube axis and Re is the Reynolds number based on tube diameter and mean velocity. Dean's perturbation solution (1927, 1928) is valid for small values of D. The numerical solutions of McConalogue & Srivastava (1968) and Truesdell & Adler (1970) describe the moderate Dean number flow field, while the asymptotic boundary-layer analyses of Barua (1963) and Mori & Nakayama (1965) are applicable at large Dean numbers.

In contrast to the steady flow situation, the problem of unsteady flow in a curved tube has been, for the most part, ignored. This paper treats the problem of pulsating flow under the influence of a pressure gradient oscillating at frequency ω. Since this study was completed, a parallel effort by Lyne (1970) has appeared. Lyne has treated the case where the frequency parameter $\omega a^2/\nu$ is large and the parameter $K^2/(Ra\omega^4)$ is small. Here K is proportional to the pressure-gradient amplitude and ν is the kinematic viscosity of the fluid. The present

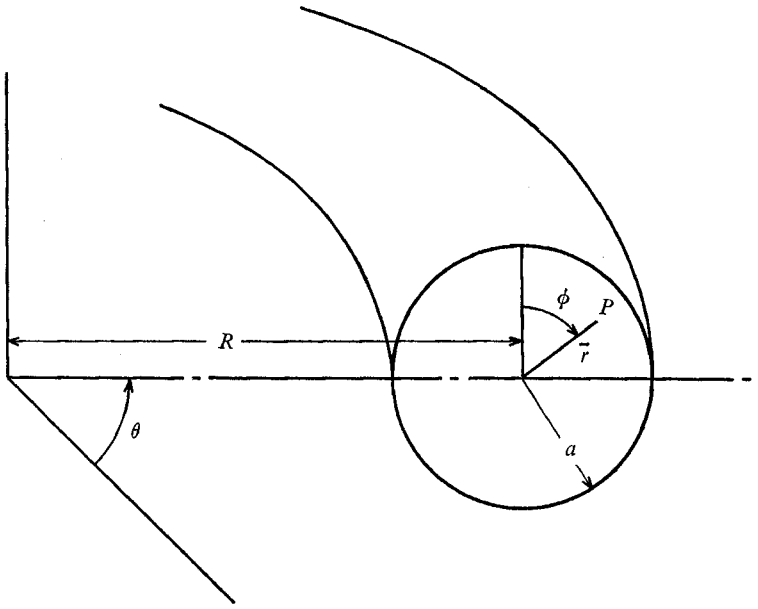

FIGURE 1. Toroidal co-ordinate system.

analysis, which follows the lines of Dean's (1927, 1928) perturbation solution for steady flow, deals with small, moderate and large values of the frequency parameter, but is restricted to small values of the amplitude parameter

$$(a/R)\,[Ka/\omega\nu]^2.$$

2. Governing equations

It is convenient to write the equations of motion in the toroidal co-ordinate system $(\bar{r}, \phi, \theta)$ illustrated in figure 1. A cross-section in the tube is located by the angle θ, measured from some reference axis. A point P in the cross-section is located by the polar co-ordinates $\bar{r}$ and ϕ. The radius of curvature of the tube axis is denoted by R.

The $(\bar{r}, \phi, \theta)$ components of velocity are denoted by (U, V, W). The assumption of fully developed flow dictates that all three velocity components be independent of θ.

The continuity equation for incompressible flow,

$$\frac{\partial}{\partial \bar{r}}(\bar{r}RU) + \frac{\partial}{\partial \phi}(RV) = 0, \tag{2.1}$$

can be identically satisfied through the introduction of a stream function $\overline{\psi}$ such that

$$U = \frac{1}{R\bar{r}}\frac{\partial \overline{\psi}}{\partial \phi}, \quad V = -\frac{1}{R}\frac{\partial \overline{\psi}}{\partial \bar{r}}. \tag{2.2}$$

The governing equations for $\overline{\psi}$ and the axial velocity function $\Omega = RW$ are the axial component of the vorticity equation (Goldstein 1938),

$$\bar{r}(R+\bar{r}\sin\phi)^2\frac{\partial}{\partial\bar{t}}(D^2\overline{\psi})+2\Omega\left[\bar{r}\cos\phi\frac{\partial\Omega}{\partial\bar{r}}-\sin\phi\frac{\partial\Omega}{\partial\phi}\right]$$
$$-\left[\frac{\partial\overline{\psi}}{\partial\bar{r}}\frac{\partial}{\partial\phi}(D^2\overline{\psi})-\frac{\partial\overline{\psi}}{\partial\phi}\frac{\partial}{\partial\bar{r}}(D^2\overline{\psi})\right](R+\bar{r}\sin\phi)+2D^2\overline{\psi}\left[\bar{r}\cos\phi\frac{\partial\overline{\psi}}{\partial\bar{r}}-\sin\phi\frac{\partial\overline{\psi}}{\partial\phi}\right]$$
$$=\nu\bar{r}(R+\bar{r}\sin\phi)^2D^4\overline{\psi}, \quad (2.3)$$

and the θ component of momentum equation,

$$\frac{\partial\Omega}{\partial\bar{t}}+\frac{1}{\bar{r}(R+\bar{r}\sin\phi)}\left[\frac{\partial\overline{\psi}}{\partial\phi}\frac{\partial\Omega}{\partial\bar{r}}-\frac{\partial\overline{\psi}}{\partial\bar{r}}\frac{\partial\Omega}{\partial\phi}\right]-\nu D^2\Omega=-\frac{1}{\rho}\frac{\partial P}{\partial\theta}. \quad (2.4)$$

The notation

$$D^2=\frac{R+\bar{r}\sin\phi}{\bar{r}}\left[\frac{\partial}{\partial\bar{r}}\left(\frac{\bar{r}}{R+\bar{r}\sin\phi}\frac{\partial}{\partial\bar{r}}\right)+\frac{\partial}{\partial\phi}\left(\frac{1}{\bar{r}(R+\bar{r}\sin\phi)}\frac{\partial}{\partial\phi}\right)\right]$$

has been employed in writing the above equations. The associated boundary conditions are the requirements that all three velocity components must vanish on the tube wall. Thus

$$\partial\overline{\psi}/\partial\phi=\partial\overline{\psi}/\partial\bar{r}=\Omega=0 \quad \text{at} \quad \bar{r}=a.$$

The set of equations (2.3) and (2.4) can be simplified by restricting the analysis to only slightly curved tubes. That is, when $R\gg a$, the approximations

$$R+\bar{r}\sin\phi\approx R \quad \text{and} \quad D^2\approx\nabla^2,$$

where ∇^2 is the ordinary harmonic operator in polar co-ordinates, can be invoked.

The pressure gradient in (2.4) is assumed to vary sinusoidally with time. Hence

$$-(\rho R)^{-1}\partial P/\partial\theta=K\cos\omega\bar{t},$$

where the amplitude K is a prescribed constant.

At this point, the variables can be non-dimensionalized as follows:

$$r=\frac{\bar{r}}{a}, \quad t=\omega\bar{t}, \quad \psi=\frac{\overline{\psi}}{a\nu}, \quad w=\frac{a\Omega}{R\nu}=\frac{aW}{\nu}.$$

In terms of the non-dimensional variables, (2.3) and (2.4) become

$$\alpha^2r\frac{\partial}{\partial t}(\nabla^2\psi)+2w\left[r\cos\phi\frac{\partial w}{\partial r}-\sin\phi\frac{\partial w}{\partial\phi}\right]-\frac{a}{R}\left[\frac{\partial\psi}{\partial r}\frac{\partial}{\partial\phi}(\nabla^2\psi)-\frac{\partial\psi}{\partial\phi}\frac{\partial}{\partial r}(\nabla^2\psi)\right]$$
$$+2\left(\frac{a}{R}\right)^2\left[r\cos\phi\frac{\partial\psi}{\partial r}-\sin\phi\frac{\partial\psi}{\partial\phi}\right]\nabla^2\psi=r\nabla^4\psi \quad (2.5)$$

and

$$\alpha^2\frac{\partial w}{\partial t}+\left(\frac{a}{R}\right)\frac{1}{r}\left[\frac{\partial\psi}{\partial\phi}\frac{\partial w}{\partial r}-\frac{\partial\psi}{\partial r}\frac{\partial w}{\partial\phi}\right]-\nabla^2w=\frac{Ka^3}{\nu^2}\cos t, \quad (2.6)$$

where $\alpha^2=\omega a^2/\nu$.

The frequency parameter α^2 may be interpreted either as an oscillatory Reynolds number, or as the ratio of a characteristic diffusion time $a^2\nu^{-1}$ to a characteristic oscillation time ω^{-1}. The principal objective of this analysis is to determine the nature of the flow field at various values of α.

Since the ratio a/R has been assumed to be small, the dependent variables, ψ and w, will be expanded in a power series in a/R:

$$\left.\begin{aligned} \psi &= \psi_0 + \frac{a}{R}\psi_1 + \left(\frac{a}{R}\right)^2 \psi_2 + \ldots, \\ w &= w_0 + \frac{a}{R} w_1 + \left(\frac{a}{R}\right)^2 w_2 + \ldots. \end{aligned}\right\} \tag{2.7}$$

It is understood that the coefficients in (2.7) are actually functions of the independent variables r, ϕ and t and the frequency parameter α.

Substitution of (2.7) into (2.5) and (2.6), and the collection of terms with common powers of a/R, leads to the following set of linear equations:

$$\alpha^2 \frac{\partial w_0}{\partial t} - \nabla^2 w_0 = \frac{Ka^3}{\nu^2} \cos t, \tag{2.8}$$

$$\alpha^2 \frac{\partial}{\partial t}(\nabla^2 \psi_0) - \nabla^4 \psi_0 = -\frac{2w_0}{r}\left[r \cos\phi \frac{\partial w_0}{\partial r} - \sin\phi \frac{\partial w_0}{\partial \phi}\right], \tag{2.9}$$

$$\alpha^2 \frac{\partial w_1}{\partial t} - \nabla^2 w_1 = -\frac{1}{r}\left[\frac{\partial \psi_0}{\partial \phi}\frac{\partial w_0}{\partial r} - \frac{\partial \psi_0}{\partial r}\frac{\partial w_0}{\partial \phi}\right]. \tag{2.10}$$

The solutions to (2.8)–(2.10) will provide a first-order estimate of the secondary flow and the axial velocity.

3. Methods of solution

3.1. *Hankel transform solution*

Equation (2.8) represents the momentum equation for flow in a straight tube subjected to a sinusoidally oscillating pressure gradient. The well-known solution (Schlichting 1960, p. 419) can be written as

$$w_0 = [Ka/\omega\nu]\{B \cos t + (1-A)\sin t\}, \tag{3.1}$$

where

$$B = \frac{\mathrm{bei}\,(\alpha)\,\mathrm{ber}\,(\alpha r) + \mathrm{ber}\,(\alpha)\,\mathrm{bei}\,(\alpha r)}{\mathrm{bei}^2(\alpha) + \mathrm{ber}^2(\alpha)}$$

and

$$A = \frac{\mathrm{ber}\,(\alpha)\,\mathrm{ber}\,(\alpha r) + \mathrm{bei}\,(\alpha)\,\mathrm{bei}\,(\alpha r)}{\mathrm{bei}^2(\alpha) + \mathrm{ber}^2(\alpha)}.$$

Substitution of (3.1) into the right-hand side of (2.9) reveals that the secondary flow is composed of a steady part ψ_{00} and a part ψ_{02} that varies as e^{2it}. The governing equations for these two components are

$$\nabla^4 \psi_{00} = \left[\frac{Ka}{\omega\nu}\right]^2 \left[B\frac{dB}{dr} - (1-A)\frac{dA}{dr}\right] \cos\phi \tag{3.2}$$

and

$$\nabla^4 \psi_{02} - 2i\alpha^2 \nabla^2 \psi_{02} = \left[\frac{Ka}{\omega\nu}\right]^2 \left\{B\frac{dB}{dr} + (1-A)\frac{dA}{dr} + i\left[B\frac{dA}{dr} - (1-A)\frac{dB}{dr}\right]\right\} \cos\phi. \tag{3.3}$$

These equations are amenable to solutions of the form

$$\psi_{00} = [Ka/\omega\nu]^2 F_0(r)\cos\phi, \quad \psi_{02} = [Ka/\omega\nu]^2 F_2(r)\cos\phi.$$

The original boundary conditions on ψ now require that

$$F_0 = dF_0/dr = F_2 = dF_2/dr = 0 \quad \text{at} \quad r = 1. \tag{3.4}$$

The appearance of the biharmonic and Laplacian operators in (3.2) and (3.3) suggests that Hankel transforms may provide a convenient means for solving for F_0 and F_2. The finite domain and homogeneous boundary conditions lend themselves to the finite Hankel transform introduced by Sneddon (1951, p. 82):

$$\bar{F}(\xi_j) = \int_0^1 F(r) J_1(\xi_j r) r \, dr. \tag{3.5}$$

The inversion formula is

$$F(r) = 2 \sum_{j=1}^{\infty} \left\{ \frac{\bar{F}(\xi_j) J_1(\xi_j r)}{[J_0(\xi_j)]^2} \right\}, \tag{3.6}$$

where ξ_j denotes the jth root of $J_1(x) = 0$.

When the Hankel transform is applied to (3.2) and (3.3), the complicated terms on the right-hand side of the equations cannot be evaluated analytically. Therefore, the transformed solutions for F_0 and F_2 have been computed and inverted numerically using a Gaussian quadrature formula to evaluate the integrals. The details of the solution can be found in Zalosh (1970).

The resulting expression for ψ_0 is

$$\psi_0 = [Ka/\omega\nu]^2 [F_0 + F_{2R} \cos 2t - F_{2I} \sin 2t] \cos\phi, \tag{3.7}$$

where F_{2R} and F_{2I} are the real and imaginary parts of F_2. Equations (3.1) and (3.7) can now be used to evaluate the right-hand side of (2.10). The ensuing equation for w_1 is

$$\begin{aligned} \nabla^2 w_1 - \alpha^2 \frac{\partial w_1}{\partial t} = \left[\frac{Ka}{\omega\nu}\right]^3 \Bigg\{ & \left(2F_0 \frac{dB}{dr} + F_{2R} \frac{dB}{dr} + F_{2I} \frac{dA}{dr}\right) \cos t \\ & - \left(2F_0 \frac{dA}{dr} - F_{2R} \frac{dA}{dr} + F_{2I} \frac{dB}{dr}\right) \sin t + \left(F_{2R} \frac{dB}{dr} - F_{2I} \frac{dA}{dr}\right) \cos 3t \\ & - \left(F_{2R} \frac{dA}{dr} + F_{2I} \frac{dB}{dr}\right) \sin 3t \Bigg\} \frac{\sin\phi}{2r}. \end{aligned} \tag{3.8}$$

The t and ϕ variations on the right-hand side of (3.8) suggest a solution for w_1 of the form

$$w_1 = \tfrac{1}{2}[Ka/\omega\nu]^3 \sin\phi \, Re\{G_1(r) e^{it} + G_3(r) e^{3it}\}. \tag{3.9}$$

When (3.9) is substituted into (3.8), two linear ordinary differential equations for G_1 and G_3 are obtained. These equations have also been solved numerically using finite Hankel transforms in the same manner as for F_0 and F_2.

The numerical solutions produced consistent results at low and moderate frequencies of oscillation, but difficulties were encountered at high frequencies. These difficulties were due to a lack of convergence in the inversion formulae for the Hankel transforms at values of α higher than about 8. The series may be semiconvergent at large values of α, or the divergence may be due to numerical errors arising in the evaluation of highly oscillatory integrals. At any rate, the following approximate solution is proposed for high frequencies.

3.2. *Boundary-layer approximations*

At large frequencies, the exact solution (3.1) for pulsating flow in a straight pipe indicates that the flow field consists approximately of a uniform inviscid central core together with a viscous boundary layer adjacent to the wall. The appearance of a boundary layer suggests that boundary-layer-type approximations can be used to simplify the governing equations and obtain closed-form solutions.

Lyne (1970) developed solutions to (2.5) and (2.6) for the high frequency regime through the use of matched asymptotic expansions in inverse powers of α. Comparison with Lyne's analysis is facilitated when Lyne's characteristic velocity $\overline{W}$ is identified with K/ω. Thus, in Lyne's notation, the present work is restricted to small values of R_s, where

$$R_s = \frac{a\overline{W}^2}{R\omega\nu} = \frac{a}{R}\left(\frac{K^2}{\omega^3\nu}\right).$$

On the other hand, Lyne's solutions are applicable for both R_s small and R_s large, providing $\alpha \gg 1$ and $\overline{W}^2/Ra\omega^2$ is small.

The approach that is adopted here is to simplify (2.8)–(2.10) further by employing the approximation $\partial/\partial r \gg 1/r$ in the boundary layer. Solutions to the resulting boundary-layer equations are matched to inviscid core solutions.

For the zeroth-order axial velocity distribution this approach leads to the boundary-layer solution

$$w_0 = \mathrm{Re}\left\{i\,e^{it}\left[\frac{\sinh(i^{\frac{1}{2}}\alpha r)}{\sinh(i^{\frac{1}{2}}\alpha)} - 1\right]\right\}\left[\frac{Ka}{\omega\nu}\right], \tag{3.10}$$

which, in the core, becomes

$$\lim_{r\to 0} w_0 = [Ka/\omega\nu]\sin t. \tag{3.11}$$

The secondary-flow stream function at large α is of the form

$$\psi_0(r,\phi,t) = \cos\phi\{F_0(r) + \mathrm{Re}\,[e^{2it}F_2(r)]\}\,[Ka/\omega\nu]^2, \tag{3.12}$$

where F_0 and F_2 are given by

$$F_0(r) = \alpha^{-3}\left[c_1 x + c_3 x^3 + \frac{2^{\frac{1}{2}}}{16}\frac{\sinh 2x}{\sinh^2(\alpha/2^{\frac{1}{2}})} - \frac{\sinh x\cos(\beta+x)}{\sinh(\alpha/2^{\frac{1}{2}})}\right],$$

where $$x = \frac{\alpha r}{2^{\frac{1}{2}}},\quad \beta = \frac{\pi}{4} - \frac{\alpha}{2^{\frac{1}{2}}},\quad c_1 = \frac{2^{\frac{1}{2}}}{8} - \frac{15}{8\alpha},\quad c_3 = \frac{5}{4\alpha^3} - \frac{2^{\frac{1}{2}}}{4\alpha^2},$$

and $$F_2(r) = \alpha^{-3}\left[\frac{e^{i(\beta+x)}\sinh x}{\sinh(\alpha/2^{\frac{1}{2}})} + \frac{e^{i(\beta'+2x)}\sinh(2x)}{16\sinh^2(\alpha/2^{\frac{1}{2}})} + a_1 x + a_2\sinh(2\,i^{\frac{1}{2}}x)\right],$$

where

$$\beta' = \tfrac{1}{4}\pi - 2^{\frac{1}{2}}/\alpha,$$

$$a_1 = (\tfrac{5}{4} - \tfrac{9}{8}2^{\frac{1}{2}})\,(\alpha + i(\alpha-1))/2^{\frac{1}{2}}(\alpha-\tfrac{1}{2})^2,$$

$$a_2 = -(\sinh\alpha)\,e^{-(\frac{1}{4}\pi-\alpha)}\left\{\left[\left(\frac{5}{4}\frac{\alpha}{2^{\frac{1}{2}}} - \frac{9}{16}\right)(\alpha-\tfrac{1}{2}) - \tfrac{9}{32}\right] + i\left[\tfrac{9}{16}(\alpha-\tfrac{1}{2}) - \left(\frac{5\alpha}{8\,2^{\frac{1}{2}}} - \frac{9}{32}\right)\right]\right\}\Big/(\alpha-\tfrac{1}{2})^2.$$

It is possible to use boundary-layer approximations to seek solutions of the higher order equations in the perturbation scheme, but cumbersome algebra makes this prospect unappealing.

3.3. *Quasi-steady approximation*

The case of low frequency flow (small α) also lends itself to a closed-form solution. A low frequency approximation for w_0 can be obtained by expanding (3.1) in a power series in αr. Power series expressions for the ber and bei functions lead to the result

$$w_0 = [Ka^3/\nu^2]\{\tfrac{1}{4}(1-r^2)\cos t + \tfrac{1}{64}\alpha^2(3-4r^2+r^4)\sin t + O(\alpha^4)\}. \tag{3.13}$$

The first term in (3.20) is recognizable as the parabolic velocity profile in phase with the applied pressure gradient. The second term represents a first-order correction for inertial effects, and manifests itself as a slight phase lag. A comparison between (3.13) and the exact solution (3.1) at $\alpha = 2$ indicates that the low frequency approximation deviates from the exact solution by less than 5 %. Of course, lower values of α produce better accuracy.

If (3.13) is used to evaluate the right-hand side of (2.9), a low frequency solution for ψ_0 should be of the form

$$\psi_0 = \psi_{00} + \alpha^2\psi_{02} + O(\alpha^4). \tag{3.14}$$

When terms with like powers of α are collected in (2.9), the solutions

$$\psi_{00} = -\left[\frac{Ka^3}{4\nu^2}\right]^2 \frac{\cos\phi}{72} r(1-r^2)^2\left(1-\frac{r^2}{4}\right)\cos^2 t \tag{3.15}$$

and

$$\psi_{02} = -[Ka^3/4\nu^2]^2\cos\phi\sin 2t[1475r - 3435{\cdot}5r^3 + 2500r^5 - 592{\cdot}5r^7 + 52r^9 + r^{11}]/(288\times 960) \tag{3.16}$$

are obtained.

The first-order axial velocity can be found from (2.10) with the right-hand side evaluated from (3.13), (3.15) and (3.16).

Following the same approach as for w_0 and ψ_0, a solution for w_1 of the form

$$w_1 = w_{10} + \alpha^2 w_{12} + O(\alpha^4) \tag{3.17}$$

is assumed. When (3.17) is substituted into (3.16), and terms with like powers of α are segregated, two quasi-steady equations for w_{10} and w_{12} are established. The solutions are

$$w_{10} = [Ka^3/4\nu^2]^3 F_{10}(r)\sin\phi\cos^3 t, \tag{3.18}$$

where $$F_{10}(r) = (19r - 40r^3 + 30r^5 - 10r^7 + r^9)/720\times 16,$$

and

$$w_{12} = [Ka^3/4\nu^2]^3 F_{12}(r)\sin\phi\sin t\cos^2 t, \tag{3.19}$$

where

$$F_{12}(r) = \left(134r - \frac{2238r^3}{8} + 218r^5 - \tfrac{515}{6}r^7 + 14{\cdot}9r^9 - \tfrac{1243}{120}r^{11}\right)\Big/[72\times 960].$$

Equation (3.18) is identical to Dean's first-order axial velocity (except for the $\cos^3 t$ factor), whereas (3.19) represents an unsteady correction at low frequencies.

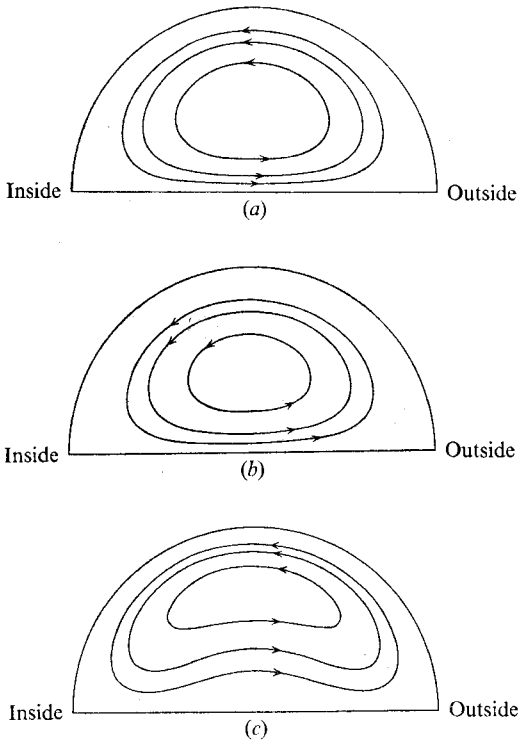

FIGURE 2. Secondary-flow streamlines at $t = 0$. (a) $\alpha = 1$. (b) $\alpha = 5$. (c) $\alpha = 10$.

4. Results

Examination of the solutions in the preceding sections indicates that the expansion parameter is actually $(a/R)\,[Ka/\omega\nu]^2$ or, if the frequency is suppressed, $(a/R)\,[Ka^3/\nu^2]^2$, and not the simple geometric ratio a/R that was implied in § 2. If K/ω is interpreted as a characteristic axial velocity, $(a/R)\,[Ka/\omega\nu]^2$ plays the role of an unsteady Dean number. The results presented here should be limited to small values of $(a/R)\,[Ka^3/\nu^2]$, with the limiting value dependent on the frequency.

An indication of the nature of the secondary flow at various frequencies can be ascertained from the streamline patterns. The solutions for the secondary-flow stream function allow the streamlines to be drawn at a prescribed time during the cycle. This has been done by linking the output of a CDC 3300 computer to a Calcomp plotter. The results are illustrated in figures 2 (a), (b) and (c) for low, moderate and high frequencies, respectively.

The low frequency and moderate frequency streamline patterns are reminiscent of the low Dean number steady flow field. The situation at high frequencies is markedly different. The streamlines are elongated and are concave downwards towards the interior. The change in streamline shape at high frequencies occurs because the tangential velocity becomes much larger than the radial velocity throughout most of the cross-section.

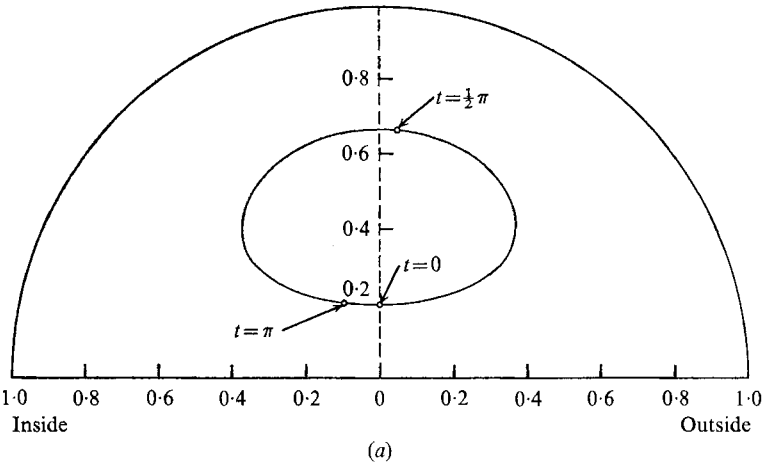

(*a*)

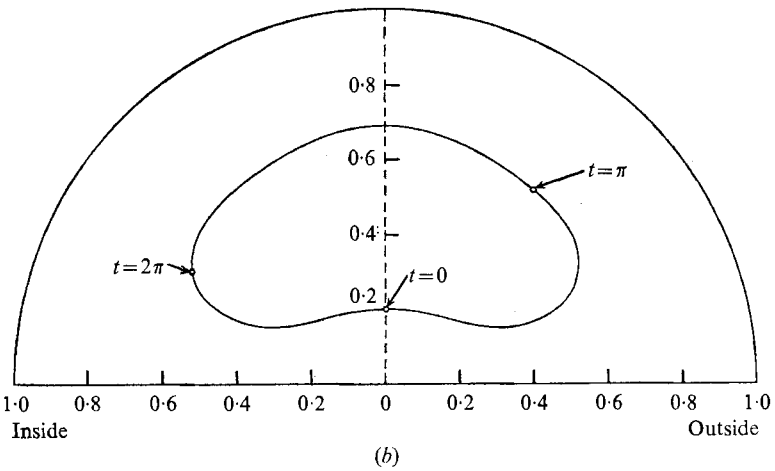

(*b*)

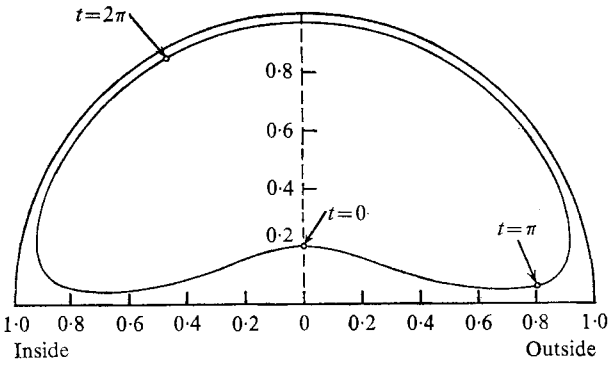

(*c*)

FIGURE 3. Particle paths. (*a*) $\alpha = 1$, $(a/R)\,[Ka^3/\nu^2]^2 = 1600$, traverse time $= 1{\cdot}04\pi$. (*b*) $\alpha = 5$, $(a/R)\,[Ka^3/\nu^2]^2 = 7{\cdot}8 \times 10^4$, traverse time $= 2{\cdot}60\pi$. (*c*) $\alpha = 10$, $(a/R)\,[Ka^3/\nu^2]^2 = 10^9$, traverse time $= 3{\cdot}52\pi$.

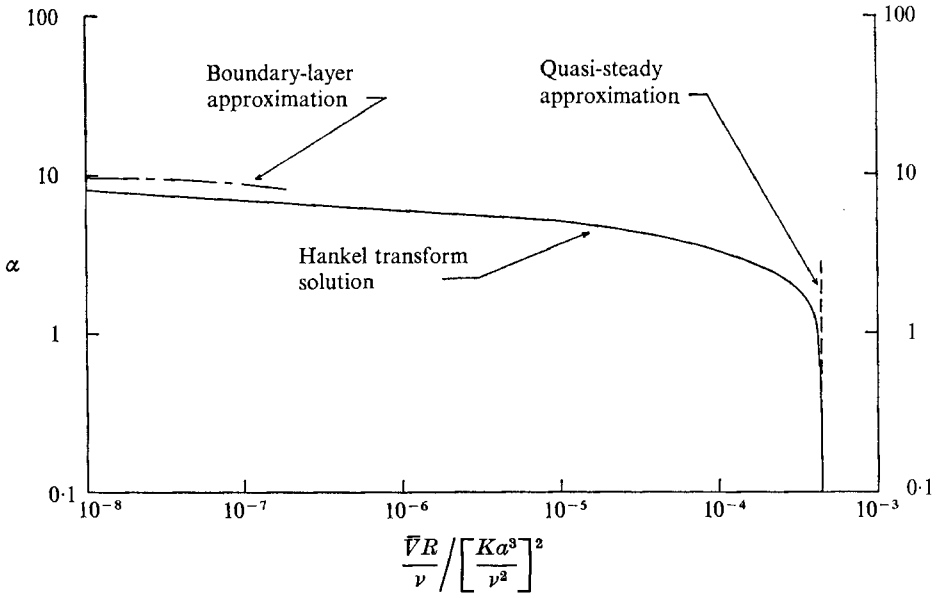

FIGURE 4. Average secondary velocity at centre of cross-section as a function of α.

The differences between the secondary flow field in the various frequency regimes is also evident from the particle path projections in the plane of the cross-section. The secondary-flow particle paths were obtained by numerically integrating the equations

$$d\bar{r}/d\bar{t} = U, \quad d\phi/d\bar{t} = V/\bar{r},$$

where U and V are obtained by differentiating the solutions for the secondary-flow stream function according to (2.2). The path of a particle originally located at the point $r = 0{\cdot}2$, $\phi = 0$ has been drawn in figures 3 (a), (b) and (c) for values of α of 1, 5 and 10 respectively. The value of the parameter $(a/R)\,[Ka^3/\nu^2]^2$ was chosen so as to complete the path in a reasonable amount of computation time without sacrificing accuracy, larger values of $(a/R)\,[Ka^3/\nu^2]^2$ being required at high frequencies. The paths reveal that a particle near the interior of the cross-section will migrate quite close to the wall at high frequencies.

For a given value of $(a/R)\,[Ka^3/\nu^2]^2$, the magnitude of the secondary velocities decreases sharply with increasing frequency. This trend is illustrated in figure 4, where the time-averaged secondary velocity at the centre of the cross-section is plotted as a function of the frequency parameter α. Both the Hankel transform solution and the boundary-layer approximation predict a reversal of flow at the centre of the cross-section at high frequencies. That is, the secondary flow is directed toward the centre of curvature, in contrast to the steady flow and low frequency situation. The flow reversal occurred at a value of α of about 9 with the Hankel transform solution and 10 with the boundary-layer approximation. This phenomenon also resulted from Lyne's solution (1970).

A physical explanation for the flow reversal can be obtained from a glance at the axial velocity profiles. Velocity profiles across the diameter $\phi = \frac{1}{2}\pi, \frac{3}{2}\pi$ lying

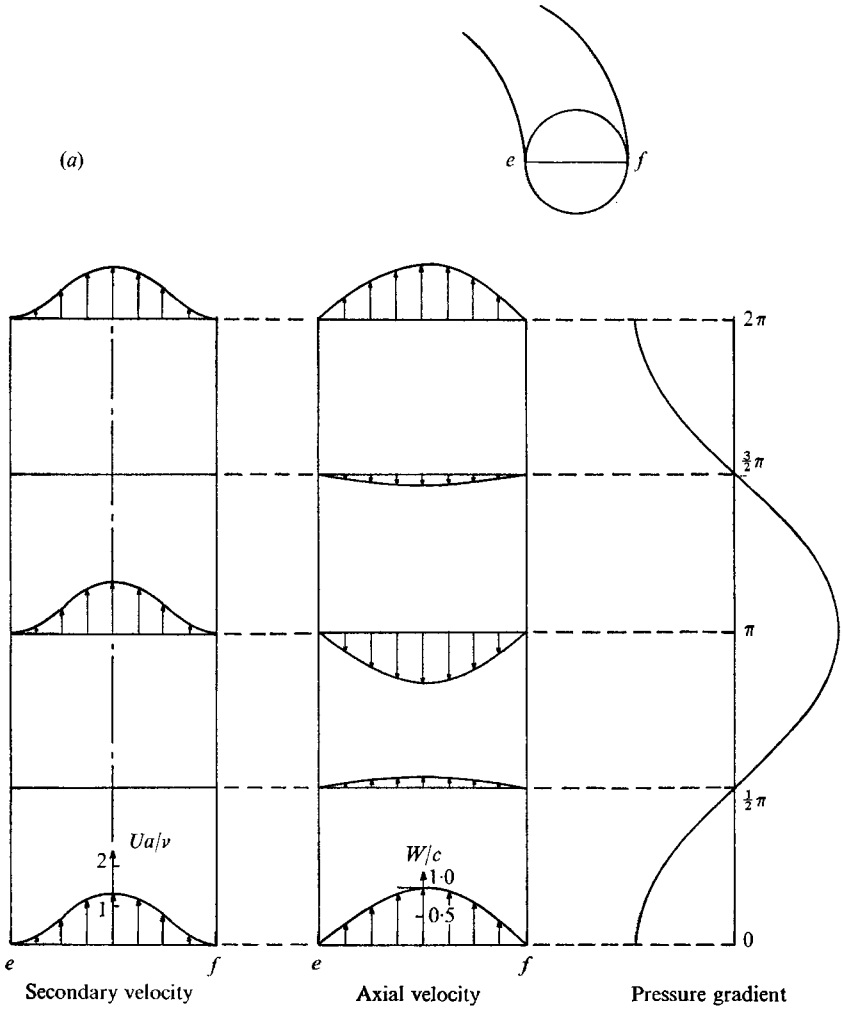

FIGURE 5 (*a*). For legend see page 704.

in the plane of the pipe axis are illustrated in figure 5 (*a*) for $\alpha = 1$. The sinusoidally varying pressure gradient is plotted alongside the profiles so that the phase relationships can be appreciated. At low frequencies, the velocities appear to be in phase with the applied pressure gradient.

Axial velocities are largest near the centre of the cross-section, although they are slightly larger on the outer portion of the diameter. Consequently, the centrifugal force is largest near the pipe axis. The centrifugal-force gradient $2w\cos\phi(\partial w/\partial r)$ is the driving force for the secondary motion that develops within the cross-section. At low frequencies, the centrifugal-force gradient drives the fluid towards the outer wall along a horizontal diameter.

The high frequency picture (figure 5 (*b*)) is quite different. There is a double off-axis peak in the axial velocity, and the centrifugal-force gradient is opposite in sign from the low frequency situation. Consequently, the secondary flow is

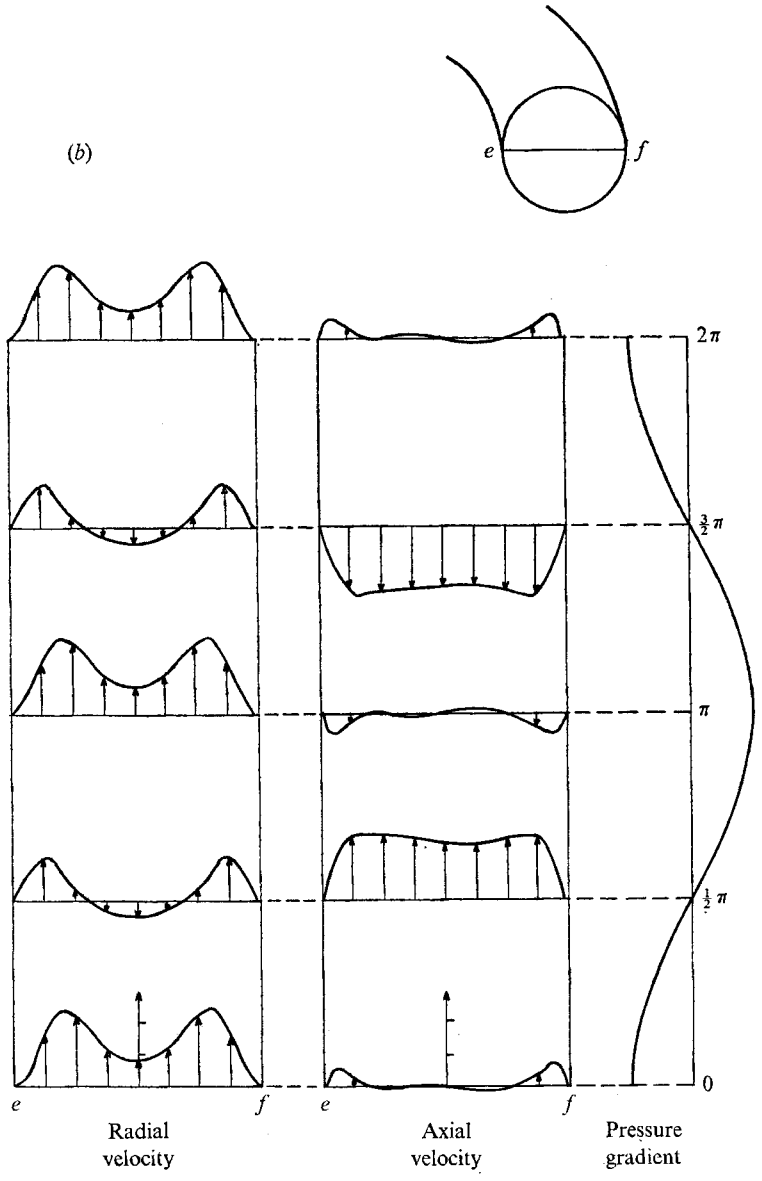

FIGURE 5. Velocity profiles across the horizontal diameter $\phi = \frac{1}{2}\pi, \frac{3}{2}\pi$. (*a*) $\alpha = 1$, $(a/R)[Ka^3/\nu^2]^2 = 1600$, $c = Ka^2/4\nu$. (*b*) $\alpha = 10$, $(a/R)[Ka/\omega\nu]^2 = 2 \times 10^3$, $c = Ka^2/100\nu$, c', $10^{-4}(\nu/R)[Ka/\omega\nu]^2$.

in the opposite direction, towards the inner wall. This type of flow pattern has been observed experimentally by Drinker *et al.* (1969) and Lyne (1970).

Figure 5(*b*) also indicates that the axial velocity lags behind the pressure gradient by one quarter of a cycle. A similar phase relationship exists for the axial velocity profile along the vertical diameter $\phi = 0$, π (not illustrated), although the asymmetry due to curvature is not present. The secondary velocity

profiles in figure 5(*b*) exhibit a region of flow reversal at $t = \frac{1}{2}\pi, \frac{3}{2}\pi$ that is not present at $t = 0, \pi$. The fact that the secondary flow varies at twice the frequency of the applied pressure gradient is also evident from figure 5.

5. Summary and conclusions

Three different solutions for fully developed pulsating flow in a curved tube have been presented. The solutions, which are restricted to small values of $(a/R)\,[Ka/\omega\nu]^2$, span the range from small to large values of α.

The results reveal that the secondary flow is composed of a steady component and a component oscillating at the second harmonic of the applied pressure gradient. Both of these components decrease rapidly in magnitude with increasing α. When α is less than about two, the streamlines and particle paths are almost identical to the low Dean number steady flow pattern. At large values of α, the streamlines become concave–convex and a fluid particle initially near the tube axis migrates close to the tube wall. Thus, the secondary-flow convective mixing is of greater extent at high frequencies because of the large excursions of fluid particles, but of lower intensity because of the smaller velocities. Consequently, there is no clear optimum value of α for possible heat- and mass-transfer applications.

The secondary-flow reversal noted by Lyne (1970) and Drinker *et al.* (1969) has also been found here for values of α larger than about 9.

For a given value of $(a/R)\,[Ka^3/\nu^2]^2$, axial velocity perturbations also decrease sharply with increasing α. The perturbations oscillate at the first and third harmonics of the pressure gradient. As in the low Dean number steady flow situation, the axial velocity perturbation varies with $\sin\phi$. Depending on the time in the cycle, the axial velocity profiles can become blunter on sharper than the straight-tube profiles.

REFERENCES

BARUA, S. N. 1963 On secondary flow in stationary curved pipes. *J. Mech. Appl. Math.* **16**, 61–77.

DEAN, W. R. 1927 Note on the motion of a fluid in a curved pipe. *Phil. Mag.* **7**, 208–223.

DEAN, W. R. 1928 The streamline motion of a fluid in a curved pipe. *Phil. Mag.* **7**, 673–695.

DRINKER, P. A., BARTLETT, R. H., BRALES, R. & NOYES, B. S. 1969 Augmentation of membrane gas transfer by induced secondary flows. *Surgery*, **66**, 775–781.

GOLDSTEIN, S. 1938 *Modern Developments in Fluid Mechanics*, vol. 1. Oxford University Press.

LYNE, W. H. 1970 Unsteady flow in a curved pipe. *J. Fluid Mech.* **45**, 13–31.

MCCONALOGUE, D. J. & SRIVASTAVA, R. S. 1968 Motion of a fluid in a curved tube. *Proc. Roy. Soc.* A **307**, 37–53.

MORI, Y. & NAKAYAMA, W. 1965 Study on forced convective heat transfer in curved pipes. *Int. J. Heat and Mass Transfer*, **8**, 67–82.

SCHLICHTING, H. 1960 *Boundary Layer Theory*, 6th edn. McGraw-Hill.

SNEDDON, I. N. 1951 *Fourier Transforms*. McGraw-Hill.

TRUESDELL, L. C. & ADLER, R. J. 1970 Numerical treatment of fully developed laminar flow in helically coiled tubes. *A.I.Ch.E. J.* **16**, 1010–1016.

ZALOSH, R. G. 1970 Pulsating flow in a curved tube. Ph.D. thesis, Northeastern University, Boston.